

Few-Shot Adversarial Low-Rank Fine-Tuning of Vision-Language Models

Sajjad Ghiasvand^{1†} Haniyeh Ehsani Oskouie^{2†}
 Mahnoosh Alizadeh¹ Ramtin Pedarsani¹
 ECE Department, UCSB¹, CS Department, UCLA²

Abstract

Vision-Language Models (VLMs) such as CLIP have shown remarkable performance in cross-modal tasks through large-scale contrastive pre-training. To adapt these large transformer-based models efficiently for downstream tasks, Parameter-Efficient Fine-Tuning (PEFT) techniques like LoRA have emerged as scalable alternatives to full fine-tuning, especially in few-shot scenarios. However, like traditional deep neural networks, VLMs are highly vulnerable to adversarial attacks, where imperceptible perturbations can significantly degrade model performance. Adversarial training remains the most effective strategy for improving model robustness in PEFT. In this work, we propose **AdvCLIP-LoRA**, the first algorithm designed to enhance the adversarial robustness of CLIP models fine-tuned with LoRA in few-shot settings. Our method formulates adversarial fine-tuning as a minimax optimization problem and provides theoretical guarantees for convergence under smoothness and nonconvex-strong-concavity assumptions. Empirical results across eight datasets using ViT-B/16 and ViT-B/32 models show that **AdvCLIP-LoRA** significantly improves robustness against common adversarial attacks (e.g., FGSM, PGD), without sacrificing much clean accuracy. These findings highlight **AdvCLIP-LoRA** as a practical and theoretically grounded approach for robust adaptation of VLMs in resource-constrained settings.

1 Introduction

Vision-Language Models (VLMs), such as CLIP [1], have become foundational in learning cross-modal representations by aligning visual and textual embeddings through large-scale contrastive pre-training [2–4]. While these models enable effective zero-shot and few-shot adaptation [5, 6], their larger transformer-based variants [7] demonstrate superior performance (e.g., CLIP’s ViT-L/14 surpasses ViT-B/16 by over 6% on ImageNet [8]). However, these large models typically contain billions of trainable parameters, making full fine-tuning (FFT) computationally expensive and inefficient, particularly for task-specific adaptations. To address this, Parameter-Efficient Fine-Tuning (PEFT) methods have gained traction, particularly in NLP, where techniques like adapters [9–11] and prompt tuning [12, 13] reduce overhead, by adding a small number of trainable parameters or trainable prompt tokens while keeping the rest of the model frozen.

[†]Equal contribution.

Among PEFT methods, Low-Rank Adaptation (LoRA) [14] offers an efficient alternative by fine-tuning only low-rank matrices, enabling single-GPU adaptation of billion-parameter models [15] while matching full fine-tuning performance [14]. Recent work by [16] employed LoRA in the context of few-shot VLMs, demonstrating improved accuracy across various tasks and models. Unlike few-shot prompt tuning [6, 17, 18], which involves computationally intensive optimization of textual prompts, or adapter-based methods [5, 19] that often demand extensive hyperparameter tuning [20], LoRA provides a more scalable and portable solution for fine-tuning VLMs [16].

Despite their impressive capabilities, VLMs share the susceptibility of traditional deep neural networks (DNNs) to adversarial attacks, where imperceptible perturbations can significantly degrade model performance [21, 22]. This vulnerability is particularly concerning in the visual domain, where adversarial noise can be more subtle and difficult to detect compared to textual modifications. Extensive research in computer vision has demonstrated that adversarial training remains the most effective approach for developing robust DNNs resistant to adversarial perturbations [23]. When applied to PEFT paradigms, this adversarial training is typically implemented during the fine-tuning phase rather than during initial pre-training. More recently, studies [24–26] have explored few-shot prompt tuning as a means of adversarial adaptation. For instance, [25] trains the clean text embedding with the adversarial image embedding to improve adversarial robustness. However, despite LoRA’s established effectiveness for standard fine-tuning tasks, its potential for enhancing adversarial robustness in VLMs remains largely unexplored. This work addresses this gap by introducing **AdvCLIP-LoRA**, a novel algorithm designed to enhance the adversarial robustness of CLIP models fine-tuned with LoRA in few-shot settings.

Before delving into the details, we summarize our main contributions. 1) We propose **AdvCLIP-LoRA**, which, to the best of our knowledge, is the first algorithm designed to enhance the adversarial robustness of CLIP models fine-tuned with LoRA in few-shot settings by formulating and solving a minimax optimization problem. 2) We provide theoretical guarantees by proving that, under assumptions of non-convex–strong-concavity and smoothness of the objective functions in our minimax formulation, the primal function defined as $\Phi(\cdot) = \max_{\delta \in \Delta} f(\cdot, \delta)$ converges to a stationary solution. 3) We conduct extensive experiments across eight datasets using ViT-B/16 and ViT-B/32 CLIP models to evaluate the effectiveness of our approach. Results demonstrate that **AdvCLIP-LoRA** significantly improves the robustness of LoRA-fine-tuned CLIP models against FGSM and PGD adversarial attacks in few-shot settings.

2 Preliminaries and Related Work

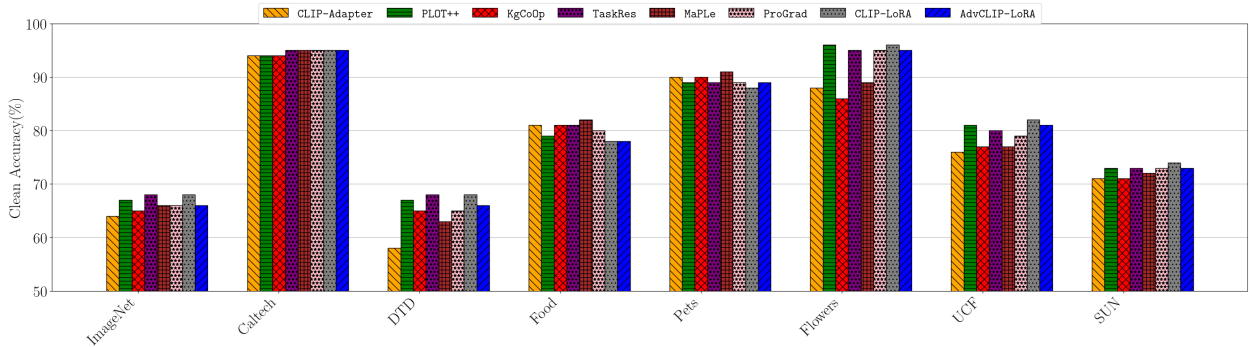
2.1 Alternative Strategies for PEFT

Prompt tuning has emerged as an alternative to weight tuning for parameter-efficient adaptation of VLMs. CoOp [27] learns continuous prompt tokens appended to class names, while CoCoOp [28] extends this by generating instance-specific prompts conditioned on images. Other variants, such as ProGrad [6] and KgCoOp [29], project prompts toward handcrafted templates to preserve pretrained knowledge. PLOT [18] jointly adapts both image and text modalities using an optimal transport objective, and MaPLe [30] further extends this by coupling interdependent prompts across vision and text encoders.

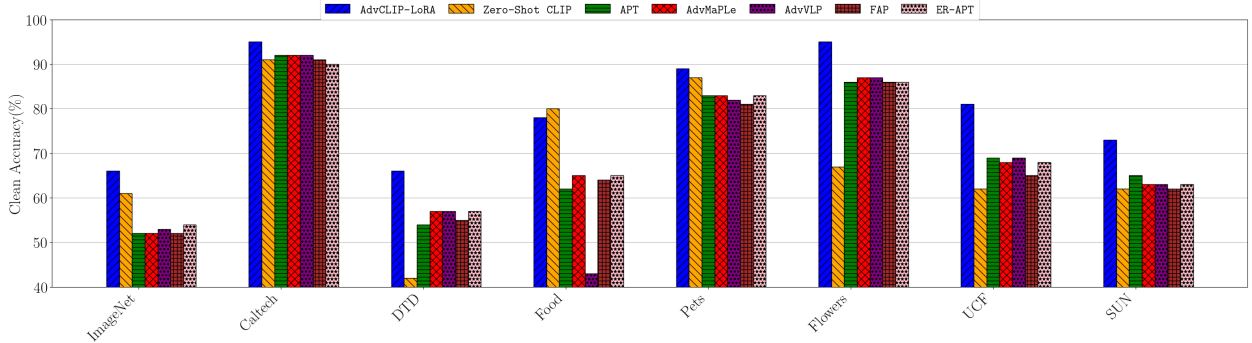
While prompt tuning is highly parameter-efficient, it can underperform in generalization [31] and scale poorly with larger datasets [16]. Moreover, as shown in [16, 32], prompt-based methods typically

require significantly longer training times compared to weight-based approaches. Given that prompt tuning is conceptually orthogonal to our LoRA-based adaptation method, we do not include direct comparisons in our main experiments. However, as shown in Fig. 1a, our method, AdvCLIP-LoRA, achieves comparable and in some cases superior clean accuracy to these non-robust prompt-tuning approaches and to standard CLIP-LoRA, despite our focus on adversarial robustness.

Adversarial Prompt Tuning. Several recent works attempt to improve the robustness of prompt-tuned VLMs. APT [24] learns robust text prompts via adversarial training, while FAP [22] leverages multimodal prompts and proposes a loss function that balances the connection between natural and adversarial features across modalities. However, these approaches suffer from reduced clean accuracy—sometimes performing worse than even zero-shot CLIP—whereas AdvCLIP-LoRA consistently outperforms them, as illustrated in Fig. 1b.



(a) AdvCLIP-LoRA vs. Non-Robust PEFT Methods (CLIP-Adapter [19], PLOT++ [18], KgCoOp [29], TaskRes [33], MaPLe [30], ProGrad [6], CLIP-LoRA [16]).



(b) AdvCLIP-LoRA vs. Robust PEFT Methods (APT [24], AdvMaPLe [30], AdvVLP [34], FAP [34], ER-APT [26]).

Figure 1: 16-shot comparison of AdvCLIP-LoRA with both non-robust and robust PEFT methods using the ViT-B/32 model across eight datasets. Results for non-robust and robust PEFT baselines are taken from [16] and [26], respectively.

2.2 Few-Shot Fine-Tuning for VLMs

In vision-language classification tasks, predictions are made by leveraging the pretrained alignment between visual and textual modalities. Given a label set of K classes, one first constructs natural language descriptions, or prompts [35], denoted as $\{c_k\}_{k=1}^K$, where each c_k is a textual phrase such as “a photo of a [class name].” These prompts are embedded using a frozen text encoder θ_t , yielding

normalized representations $\mathbf{z}_k^{(T)} = \theta_t(c_k) \in \mathbb{R}^d$. Similarly, an image \mathbf{x}_i is embedded via a visual encoder θ_v to obtain $\mathbf{z}_i^{(I)} = \theta_v(\mathbf{x}_i) \in \mathbb{R}^d$, also normalized to unit length. The prediction logits are computed as the cosine similarity between each image-text pair. These logits are converted into a probability distribution over classes using a softmax with temperature scaling:

$$p_{i,k} = \frac{\exp(\cos(\mathbf{z}_i^{(I)}, \mathbf{z}_k^{(T)})/\gamma)}{\sum_{j=1}^K \exp(\cos(\mathbf{z}_i^{(I)}, \mathbf{z}_j^{(T)})/\gamma)}, \quad (1)$$

where γ is a softmax-temperature parameter. The predicted label for image \mathbf{x}_i is the one with the highest posterior probability: $\hat{k} = \arg \max_k p_{i,k}$. This form of zero-shot prediction directly mirrors the contrastive training setup used in large-scale VLM pretraining, such as CLIP [1], and allows models to generalize to novel classification tasks without any fine-tuning on the target domain.

To further adapt vision-language models to downstream tasks, the few-shot setting assumes access to a limited number of labeled examples per target class—typically fewer than 16. Given N such labeled support images per class, we denote the one-hot encoded ground-truth label for image \mathbf{x}_i as y_{ik} , where $y_{ik} = 1$ if \mathbf{x}_i belongs to class k , and 0 otherwise. Classification probabilities $p_{i,k}$ are obtained as in the zero-shot setup, and the model is adapted by minimizing the cross-entropy loss: $\mathcal{L}_{\text{CE}} = -\frac{1}{N} \sum_{i=1}^N \sum_{k=1}^K y_{ik} \ln p_{i,k}$.

This adaptation can be implemented in several ways. One strategy is to optimize the input prompts $\{c_k\}_{k=1}^K$ directly—an approach inspired by prompt tuning techniques [18]. Alternatively, one may choose to fine-tune lightweight, task-specific modules such as adapter layers [19] or low-rank parameterizations like LoRA [16], leaving the backbone encoders frozen.

2.3 Fine-Tuning VLMs via LoRA

Low-Rank Adaptation (LoRA) [14] is a highly promising PEFT method, enabling efficient fine-tuning of large models by freezing the entire pre-trained model and introducing low-rank, trainable matrices within each layer. In LoRA, given a pre-trained weight matrix $W_0 \in \mathbb{R}^{d \times k}$, the weight update is achieved through a low-rank decomposition $W_0 + \Delta W = W_0 + BA$, where the training occurs on matrices $A \in \mathbb{R}^{r \times k}$ and $B \in \mathbb{R}^{d \times r}$, with $r \ll \min(d, k)$. The values in A are initialized randomly via a Gaussian distribution, while B is initialized as a zero matrix. This setup ensures that no low-rank update occurs before training, meaning that the output remains unchanged initially.

Although the original LoRA paper applies the low-rank matrices to the attention matrices of transformer-based architectures, [16] extends LoRA to all matrices in the vision and text encoders of VLMs. This adaptation leads to improved accuracy over prompt-based methods across various CLIP architectures and datasets [16].

2.4 Adversarial Robustness

Given an arbitrary classifier $h : \mathcal{X} \rightarrow \mathcal{Y}$, where an input $x \in \mathcal{X}$ is associated with its true label $y \in \mathcal{Y}$, an adversary attempts to find an imperceptible perturbation δ , which shares the same dimensionality as x . This perturbation must satisfy the condition that $x + \delta \in \mathcal{X}$, and more critically, $h(x + \delta) \neq y$, thereby misclassifying the original input. To ensure that this perturbation remains imperceptible, the adversarial perturbation δ is usually constrained within some bounded set $\Delta \subseteq \mathbb{R}^n$.

Algorithm 1 AdvCLIP-LoRA

```
1: Input: Learning rates  $\eta_w$  and  $\eta_\delta$ , batch-size  $M$ , number of iterations  $T$ .
2: Initialize:  $A_0 \sim \mathcal{N}(0, \sigma^2)$ ,  $B_0 = 0$ .
3: for iteration  $t \leftarrow 1$  to  $T$  do
4:   Draw a collection of i.i.d. data samples  $\{\xi_i\}_{i=1}^M$ 
5:    $\delta_t = \mathcal{P}_\Delta \left( \delta_{t-1} + \eta_\delta \left( \frac{1}{M} \sum_{i=1}^M \nabla_\delta F(W_{t-1}, \delta_{t-1}; \xi_i) \right) \right)$   $\triangleright$  Update and project the perturbation.
6:    $A_t = A_{t-1} - \eta_w \left( \frac{1}{M} \sum_{i=1}^M \nabla_A F(W_{t-1}, \delta_t; \xi_i) \right)$ 
7:    $B_t = B_{t-1} - \eta_w \left( \frac{1}{M} \sum_{i=1}^M \nabla_B F(W_{t-1}, \delta_t; \xi_i) \right)$   $\triangleright$  Update the low-rank matrices  $A$  and  $B$ .
8: end for
9: Randomly draw  $\hat{A}, \hat{B}$  from  $\{A_t, B_t\}_{t=1}^T$  at uniform.
10: Return:  $\hat{A}, \hat{B}$ .
```

The adversarial attack on a classifier h , constrained by bounded set Δ , is formulated as follows:

$$\hat{x} = x + \arg \max_{\delta \in \Delta} \mathcal{L}(h(x + \delta), y), \quad (2)$$

where \mathcal{L} is the training loss function. This formulation represents an optimization problem where the perturbation δ is chosen such that the classifier’s output is maximally disrupted while staying within a bounded set. Methods like Projected Gradient Descent (PGD) [23] are commonly employed to solve this optimization problem. Given the vulnerability of deep learning models to these perturbations [21], it becomes crucial to defend against such adversarial attacks.

One of the most effective strategies for defending against adversarial attacks is adversarial training, as proposed by [23]. When h_W denotes a classifier parameterized by W , adversarial training seeks to solve the following minimax optimization problem:

$$\min_W \mathbb{E}_{(x,y) \sim \mathcal{D}} \left[\max_{\delta \in \Delta} \mathcal{L}(h_W(x + \delta), y) \right], \quad (3)$$

where \mathcal{D} represents the underlying data distribution. This approach effectively trains the classifier to be robust against adversarial perturbations by simultaneously minimizing the classifier’s loss and maximizing the perturbation within a bounded set.

3 Proposed Algorithm

3.1 Adversarial Fine-Tuning of CLIP via LoRA

Assume that the LoRA matrices A and B are initialized with a Gaussian distribution and zero matrices, respectively, and are applied to all weight matrices in the vision and text encoders of a CLIP model. Following the approach introduced in Section 2.4, we aim to improve the adversarial robustness of the LoRA-based CLIP model by introducing a perturbation δ to input images and solving a minimax optimization problem. Focusing on the dependence of the training loss function on the low-rank matrices A and B and the perturbation δ , we formulate the following minimax optimization problem:

$$\min_{A,B} \max_{\delta \in \Delta} f(W := W_0 + BA, \delta), \quad (4)$$

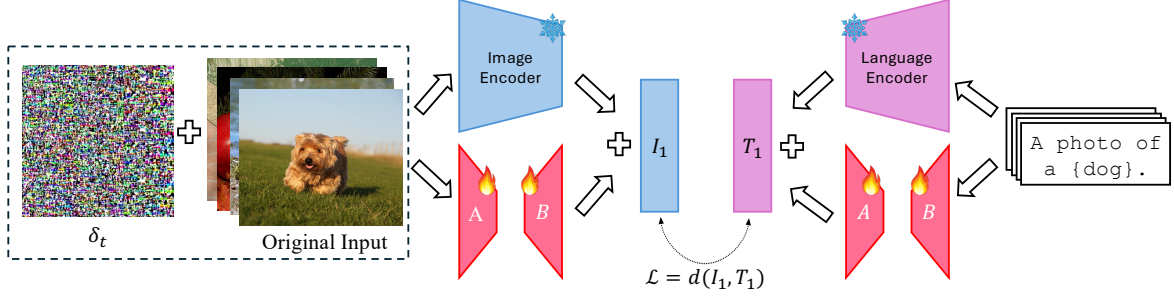


Figure 2: 🔥: Trainable Parameters, ⭐: Frozen Parameters. Illustration of AdvCLIP-LoRA algorithm. During each iteration t , the perturbation δ_t is updated and applied to the input image batch. Subsequently, the low-rank matrices A and B are optimized, while the rest of the model remains frozen.

where Δ is a bounded set of admissible perturbations, and $f : \mathbb{R}^{d \times k+n} \rightarrow \mathbb{R}$ is a non-convex loss function expressible in the stochastic form $\mathbb{E}_{\xi \sim \mathcal{D}}[F(W_0 + BA, \delta; \xi)]$. Here, the expectation is taken over randomly sampled batches $\xi \sim \mathcal{D}$, where \mathcal{D} represents the underlying data distribution.

3.2 AdvCLIP-LoRA Algorithm

In this section, we present the proposed AdvCLIP-LoRA algorithm, which solves the minimax problem (4) to enhance the adversarial robustness of a CLIP model fine-tuned with LoRA. The AdvCLIP-LoRA algorithm proceeds for T iterations. At each iteration t :

- 1) Select M independent and identically distributed (i.i.d.) samples $\{\xi_i\}_{i=1}^M$ from the dataset.
- 2) Update the perturbation δ via:

$$\delta_t = \mathcal{P}_\Delta \left(\delta_{t-1} + \frac{\eta_\delta}{M} \sum_{i=1}^M \nabla_\delta F(W_{t-1}, \delta_{t-1}; \xi_i) \right), \quad (5)$$

where η_δ is the learning rate for δ , Δ is a bounded perturbation set, and \mathcal{P}_Δ projects onto Δ .

- 3) Update the LoRA matrices A and B using the current δ_t :

$$\begin{aligned} A_t &= A_{t-1} - \eta_w \left(\frac{1}{M} \sum_{i=1}^M \nabla_A F(W_{t-1}, \delta_t; \xi_i) \right), \\ B_t &= B_{t-1} - \eta_w \left(\frac{1}{M} \sum_{i=1}^M \nabla_B F(W_{t-1}, \delta_t; \xi_i) \right), \end{aligned} \quad (6)$$

where η_w is the learning rate for A and B . In the end, the algorithm randomly draws \hat{A}, \hat{B} from $\{A_t, B_t\}_{t=1}^T$ uniformly at random.¹ The steps of the AdvCLIP-LoRA algorithm are illustrated in Fig. 2. Moreover, the AdvCLIP-LoRA pipeline can be found in Alg. 1.

¹This is a standard practice in nonconvex optimization for stochastic gradient descent to find stationary points. In practice, we select the model that achieves the highest accuracy on the validation set.

4 Convergence Analysis

In this section, we present a thorough convergence analysis of the proposed AdvCLIP-LoRA algorithm. The complete proofs can be found in Appendix B. Let us begin with a few definitions.

Definition 4.1 A function f is L -Lipschitz if for all W, W' , we have

$$\|f(W) - f(W')\| \leq L \|W - W'\|. \quad (7)$$

Definition 4.2 A function f is ℓ -smooth if for all W, W' , we have

$$\|\nabla f(W) - \nabla f(W')\| \leq \ell \|W - W'\|. \quad (8)$$

Consider the minimax problem (4), which is equivalent to minimizing the function $\Phi(\cdot) = \max_{\delta \in \Delta} f(\cdot, \delta)$. In the context of nonconvex-strongly-concave minimax problems, where $f(W, \cdot)$ is strongly-concave for each W , the maximization problem $\max_{\delta \in \Delta} f(W, \delta)$ can be solved efficiently, yielding useful insights into Φ . However, finding the global minimum of Φ remains NP-hard in general due to its nonconvex nature. To address this challenge, we define local surrogates for the global minimum of Φ . One commonly used surrogate in nonconvex optimization is the notion of stationarity, which is suitable when Φ is differentiable.

Definition 4.3 A point W is an ϵ -stationary point ($\epsilon \geq 0$) of a differentiable function Φ if $\|\nabla \Phi(W)\| \leq \epsilon$.

Let us proceed with a few assumptions. Note that $\|\cdot\|_F$ denotes the Frobenius norm.

Assumption 4.4 We assume that the stochastic gradients are unbiased and bounded, that is,

$$\mathbb{E}_\xi [\nabla F(W, \delta; \xi)] = \nabla f(W, \delta), \quad \mathbb{E}_\xi [\|\nabla F(W, \delta; \xi)\|_F^2] \leq G^2, \quad (9)$$

for all $W \in \mathbb{R}^{d \times k}$, where ξ represents a randomly sampled subset of training data and $\mathbb{E}_\xi[\cdot]$ denotes the expectation over $\xi \sim \mathcal{D}$.

Assumption 4.5 The objective function and constraint set ($f : \mathbb{R}^{d \times k + n} \rightarrow \mathbb{R}, \Delta \subseteq \mathbb{R}^n$) satisfy

1. f is ℓ -smooth and $f(W, \cdot)$ is μ -strongly concave.
2. Δ is a convex and bounded set with a diameter $D \geq 0$.

Assumption 4.6 Let $W_t = W_0 + B_t A_t$ represent the model parameters at the t -th step. For all $t = 1, \dots, T$ there exist constants $c_A > 0$ and $c_B > 0$ such that: $\|A_t\|_F \leq c_A$ and $\|B_t\|_F \leq c_B$.

We next present a proposition on the structure of the function Φ . Let $\kappa = \ell/\mu$ denote the condition number and define

$$\Phi(\cdot) = \max_{\delta \in \Delta} f(\cdot, \delta), \quad \delta^*(\cdot) = \operatorname{argmax}_{\delta \in \Delta} f(\cdot, \delta). \quad (10)$$

Proposition 4.7 [36] *Under Assumption 4.5, $\Phi(\cdot)$ is $2\kappa\ell$ -smooth with $\nabla\Phi(\cdot) = \nabla_W f(\cdot, \delta^*(\cdot))$. Also, $\delta^*(\cdot)$ is κ -Lipschitz.*

Using Proposition 4.7 and Assumption 4.6, we can prove the smoothness of $\Phi(\cdot)$ with respect to A and B when the other is held fixed. Formally, we state the following lemma:

Lemma 4.8 *Under Assumptions 4.5 and 4.6, the function $\Phi(\cdot)$ is $2\kappa\ell c_B^2$ -smooth with respect to A when B is fixed and $2\kappa\ell c_A^2$ -smooth with respect to B when A is fixed.*

Now, we present the main theoretical results using the order-wise notation for AdvCLIP-LoRA.

Theorem 4.9 *Under Assumptions 4.4, 4.5, and 4.6, and letting the learning rates be chosen as*

$$\eta_w = \Theta\left(\min\left\{\frac{1}{\kappa\ell(c_A^4 + c_B^4)}, \frac{1}{\kappa^2\ell(c_A^2 + c_B^2)}, \frac{1}{(G^2 + \kappa\ell c_A^4 c_B^2)^{1/2}}\right\}\right), \quad (11)$$

and $\eta_\delta = \Theta(1/\ell)$, the number of iterations required by AdvCLIP-LoRA to return an ϵ -stationary point is bounded by

$$\mathcal{O}\left(\frac{4\Delta_\Phi(1/\eta_w) + \kappa\ell^2(c_A^2 + c_B^2)D^2}{\epsilon^2}\right), \quad (12)$$

where $\Delta_\Phi = \mathbb{E}\Phi(W_0) - \mathbb{E}\Phi(W_{T+1})$. Moreover, the mini-batch size M is bounded by

$$\mathcal{O}\left(\frac{G^2 + \kappa(c_A^2 + c_B^2)G^2}{\epsilon^2}\right). \quad (13)$$

Remark 4.10 *First, AdvCLIP-LoRA is guaranteed to find an ϵ -stationary point of $\Phi(\cdot)$ within $\mathcal{O}(\epsilon^{-2})$ iterations and with a total stochastic gradient complexity of $\mathcal{O}(\epsilon^{-4})$. Moreover, our choice of learning rates satisfies $\eta_w \ll \eta_\delta$, which stems from the non-convex-strong-concave structure of the objective function.*

5 Empirical Results

5.1 Experiments Setup

Practical Implementation Notes for AdvCLIP-LoRA. We highlight a few minor differences between the theoretically analyzed version of AdvCLIP-LoRA and the implementation used in our experimental section. Such discrepancies are common in the literature, reflecting the gap between theoretical analysis and practical scenarios. 1) The proposed algorithm is guaranteed to visit an ϵ -stationary point within a specified number of iterations by returning \hat{A} and \hat{B} , sampled uniformly from the set $\{(A_t, B_t)\}_{t=1}^T$. However, this does not imply that the final iterate or the model achieving the best validation accuracy corresponds to the ϵ -stationary point. In our experiments, we report the test accuracy of the model that achieves the highest accuracy on the validation set. 2) At the beginning of each iteration in AdvCLIP-LoRA i.i.d. samples are drawn randomly for the dataset. However, in our implementation, we fix a minibatch and use the entire training set in every iteration. 3) As discussed in Section 3.2, AdvCLIP-LoRA updates A , B , and δ once per iteration, and we have

Table 1: Detailed results for the 8 datasets with ViT-B/16 as backbone. Top-1 accuracy averaged over 3 random seeds is reported. Highest value is highlighted in **bold**.

Shots	Method	ImageNet			Caltech			DTD			Food		
		Clean	FGSM	PGD	Clean	FGSM	PGD	Clean	FGSM	PGD	Clean	FGSM	PGD
1	CLIP-LoRA	70.24	15.14	4.73	94.20	59.86	26.26	54.77	14.99	3.11	84.99	8.43	2.90
	AdvCLIP-LoRA ($\tau = 1$)	56.02	29.17	17.10	92.67	62.70	26.40	49.64	20.09	4.06	79.86	26.50	9.62
	AdvCLIP-LoRA ($\tau = 2$)	54.76	30.52	19.44	90.20	67.29	29.48	50.53	21.12	3.04	78.19	31.31	12.74
	AdvCLIP-LoRA ($\tau = 4$)	53.14	31.19	21.70	87.17	70.18	34.16	48.84	21.16	2.60	74.88	35.01	20.04
	AdvCLIP-LoRA ($\tau = 6$)	50.19	30.96	21.30	83.96	79.69	37.09	44.71	31.86	3.17	72.09	57.40	26.45
	AdvCLIP-LoRA ($\tau = 8$)	45.35	30.60	21.66	81.39	78.96	41.28	42.61	32.76	4.24	68.57	58.32	32.84
	AdvCLIP-LoRA ($\tau = 10$)	42.88	30.12	22.38	77.51	76.54	40.76	42.12	33.35	6.14	64.52	56.22	34.47
4	CLIP-LoRA	71.52	14.59	5.12	95.16	59.39	29.19	63.73	19.39	6.68	83.07	7.83	2.21
	AdvCLIP-LoRA ($\tau = 1$)	67.81	40.62	37.74	95.28	76.84	61.49	59.73	27.64	8.89	83.75	31.57	27.47
	AdvCLIP-LoRA ($\tau = 2$)	67.63	42.53	38.42	95.15	80.68	72.81	59.26	31.01	13.59	83.77	35.19	35.03
	AdvCLIP-LoRA ($\tau = 4$)	67.43	42.50	41.40	95.20	84.00	82.80	60.40	36.41	26.04	83.67	43.52	50.08
	AdvCLIP-LoRA ($\tau = 6$)	66.90	44.35	43.75	95.19	92.03	87.21	59.75	49.45	34.71	83.53	69.85	56.92
	AdvCLIP-LoRA ($\tau = 8$)	66.67	44.47	43.92	95.03	92.67	88.27	59.42	50.87	39.54	83.12	73.09	62.16
	AdvCLIP-LoRA ($\tau = 10$)	65.93	45.15	45.07	95.03	92.66	89.36	59.60	52.42	44.48	82.56	72.74	65.41
16	CLIP-LoRA	73.41	14.56	5.51	96.31	60.63	31.05	72.40	24.57	9.30	84.32	7.15	2.45
	AdvCLIP-LoRA ($\tau = 1$)	72.03	44.41	30.24	96.19	79.92	74.13	70.51	33.06	15.78	84.77	26.43	23.41
	AdvCLIP-LoRA ($\tau = 2$)	71.96	46.91	48.73	95.95	81.35	81.12	70.45	38.00	30.99	84.70	28.42	34.18
	AdvCLIP-LoRA ($\tau = 4$)	71.69	47.42	50.08	96.09	82.14	86.31	69.70	42.61	46.02	84.24	32.68	48.56
	AdvCLIP-LoRA ($\tau = 6$)	71.32	47.44	50.34	96.08	93.12	88.95	69.31	60.26	52.27	83.68	66.18	55.57
	AdvCLIP-LoRA ($\tau = 8$)	69.63	53.31	56.33	96.16	93.72	90.82	68.93	61.43	55.70	83.05	68.12	59.64
	AdvCLIP-LoRA ($\tau = 10$)	67.00	54.71	57.56	96.09	94.28	91.98	68.28	62.61	58.69	82.75	69.25	62.17
Shots	Method	Pets			Flowers			UCF			SUN		
		Clean	FGSM	PGD	Clean	FGSM	PGD	Clean	FGSM	PGD	Clean	FGSM	PGD
1	CLIP-LoRA	92.14	23.52	17.21	82.45	6.70	3.15	75.95	18.36	2.98	70.22	17.78	6.20
	AdvCLIP-LoRA ($\tau = 1$)	90.02	23.51	17.17	70.62	26.04	5.33	66.44	29.53	8.94	61.68	35.60	17.50
	AdvCLIP-LoRA ($\tau = 2$)	88.34	40.84	16.75	69.62	30.42	6.86	63.04	31.95	10.68	61.02	39.98	20.41
	AdvCLIP-LoRA ($\tau = 4$)	82.76	41.56	16.66	66.14	36.80	8.66	58.80	35.09	16.07	60.01	39.91	24.03
	AdvCLIP-LoRA ($\tau = 6$)	78.35	40.96	17.90	62.79	39.09	8.86	54.59	37.02	18.71	58.61	41.34	27.40
	AdvCLIP-LoRA ($\tau = 8$)	73.21	42.56	21.15	57.69	40.06	11.20	49.58	36.80	20.22	56.66	43.33	30.46
	AdvCLIP-LoRA ($\tau = 10$)	66.37	40.95	22.92	54.01	39.29	10.79	45.33	34.65	19.57	54.56	43.80	31.46
4	CLIP-LoRA	89.99	16.73	10.08	93.48	11.20	7.62	80.44	18.85	4.00	72.19	16.15	6.20
	AdvCLIP-LoRA ($\tau = 1$)	91.36	57.37	51.38	91.10	46.41	31.14	74.42	37.49	25.23	70.99	45.40	40.31
	AdvCLIP-LoRA ($\tau = 2$)	91.06	60.57	60.56	91.03	51.39	45.29	78.51	38.06	32.07	71.28	48.84	47.63
	AdvCLIP-LoRA ($\tau = 4$)	91.07	64.57	71.11	91.03	58.53	61.24	77.96	42.07	45.39	71.19	51.37	50.67
	AdvCLIP-LoRA ($\tau = 6$)	91.05	67.77	77.72	90.62	65.16	69.60	77.83	45.35	52.36	71.69	56.71	56.20
	AdvCLIP-LoRA ($\tau = 8$)	91.06	69.96	80.19	89.78	66.38	74.67	77.09	47.98	55.99	70.96	57.14	56.96
	AdvCLIP-LoRA ($\tau = 10$)	91.22	71.70	82.02	89.35	68.59	77.75	76.60	50.47	58.53	71.04	60.27	59.89
16	CLIP-LoRA	92.18	16.28	7.14	98.19	17.39	13.09	86.71	22.20	5.01	76.22	16.94	6.15
	AdvCLIP-LoRA ($\tau = 1$)	92.90	48.31	46.94	97.55	57.42	52.53	85.96	37.73	23.54	75.94	48.77	45.10
	AdvCLIP-LoRA ($\tau = 2$)	92.88	49.72	60.47	97.84	60.87	69.71	85.58	36.71	35.53	75.92	52.37	54.50
	AdvCLIP-LoRA ($\tau = 4$)	92.72	51.65	73.12	97.70	65.68	83.88	84.92	39.19	50.39	76.09	55.02	61.05
	AdvCLIP-LoRA ($\tau = 6$)	92.65	56.37	78.18	97.45	68.71	88.09	84.33	40.60	58.42	75.58	57.18	64.04
	AdvCLIP-LoRA ($\tau = 8$)	92.33	58.02	80.52	97.39	70.97	90.29	83.38	42.05	62.15	75.89	59.28	66.43
	AdvCLIP-LoRA ($\tau = 10$)	92.43	60.49	81.86	97.33	74.26	91.83	83.08	43.93	65.40	75.87	61.92	68.18

shown that this procedure guarantees convergence to a stationary solution. However, our empirical findings suggest that performing multiple updates and projections on δ per iteration can enhance robustness, though it may lead to a slight reduction in clean accuracy on some datasets. This gain in robustness stems from a more precise approximation of the inner maximization in the minimax formulation, allowing the model to better anticipate adversarial perturbations. We denote the number of δ -updates per iteration by τ , and conduct extensive experiments to evaluate the impact of varying τ .

Datasets. To evaluate the proposed method, we follow prior works [26, 27] and utilize a diverse set of 8 image recognition datasets spanning multiple vision tasks. The datasets include two generic object recognition datasets: ImageNet-1K [8] and Caltech101 [37]; a texture recognition dataset: DTD [38]; four fine-grained object recognition datasets: OxfordPets [39], Flowers102 [40], and Food101 [41]; a scene recognition dataset: SUN397 [42]; and an action recognition dataset: UCF101 [43].

Implementation Details. To evaluate the performance of our proposed method, we conduct

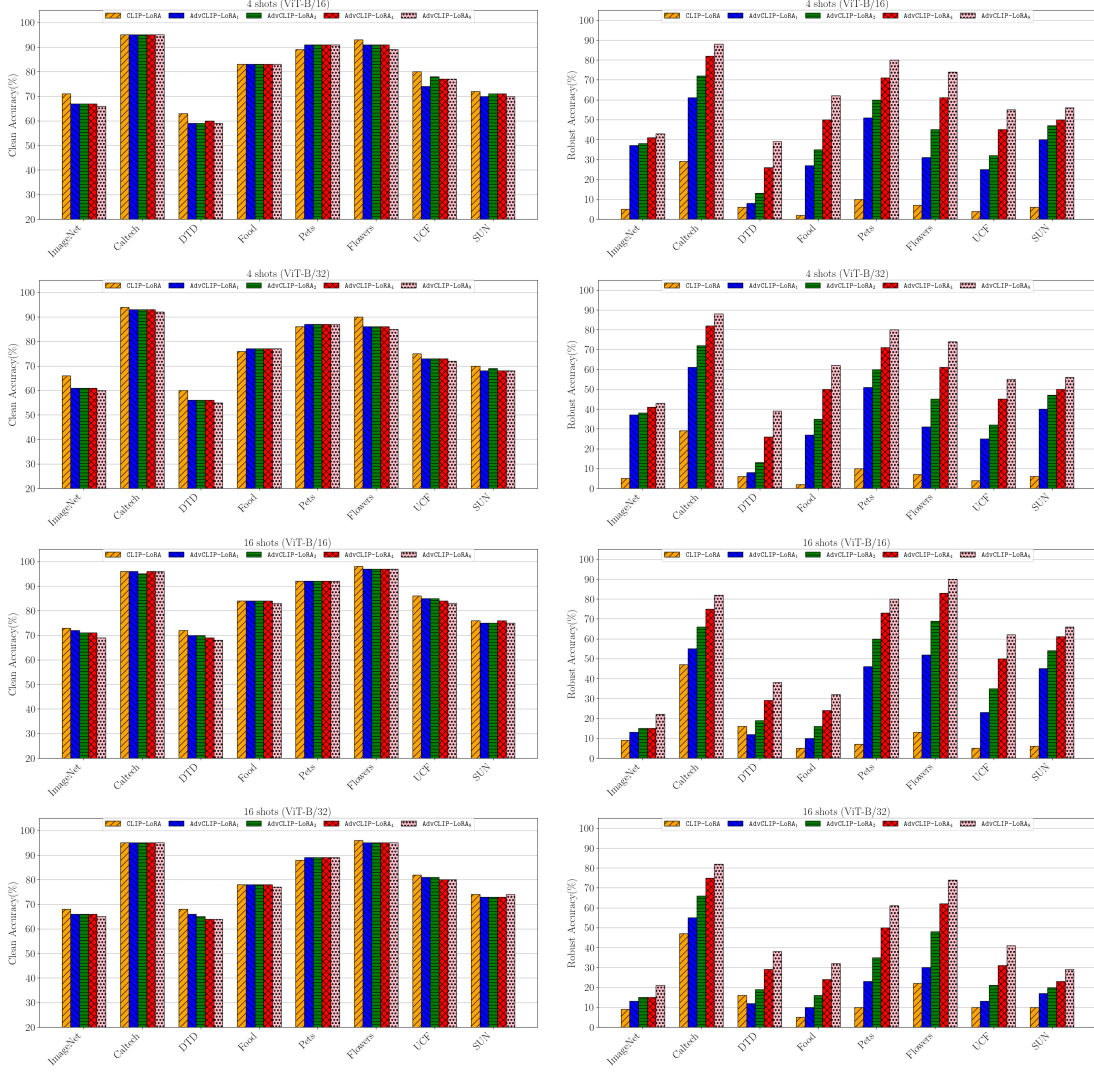


Figure 3: Comparative analysis of CLIP-LoRA and AdvCLIP-LoRA with ViT-B/16 and ViT-B/32 backbones on 8 fine-grained datasets, showing clean accuracy and PGD-adversarial robustness (shots labeled above). AdvCLIP-LoRA _{i} means AdvCLIP-LoRA with $\tau = i$.

extensive experiments comparing AdvCLIP-LoRA with CLIP-LoRA, using ViT-B/16 and ViT-B/32 backbones. Our experimental setup closely follows that of [16] to ensure a fair comparison. LoRA is applied to both the vision and text encoders of CLIP, with the rank of 2 and a dropout layer with $p = 0.25$. We use a batch size of 16 for ImageNet-1K and 32 for the other datasets. The number of training iterations is set to $500 \times N/K$. All experiments are conducted on NVIDIA A6000 and V100 GPUs.

Learning Rates. For the low-rank matrices, we use a learning rate of 2×10^{-4} with a cosine decay scheduler. Selecting an appropriate learning rate for δ posed a challenge, since the gradients for δ were too small to enable effective updates at the beginning of the training. To address this, we adopt a larger, adaptive learning rate defined as $\eta_\delta = 0.05/\|\delta_t\|_2$, which scales inversely with the magnitude of δ_t . This adjustment amplifies updates, improving early-stage learning. It can also be viewed as an implicit data augmentation strategy, introducing noise into the learning process. The learning

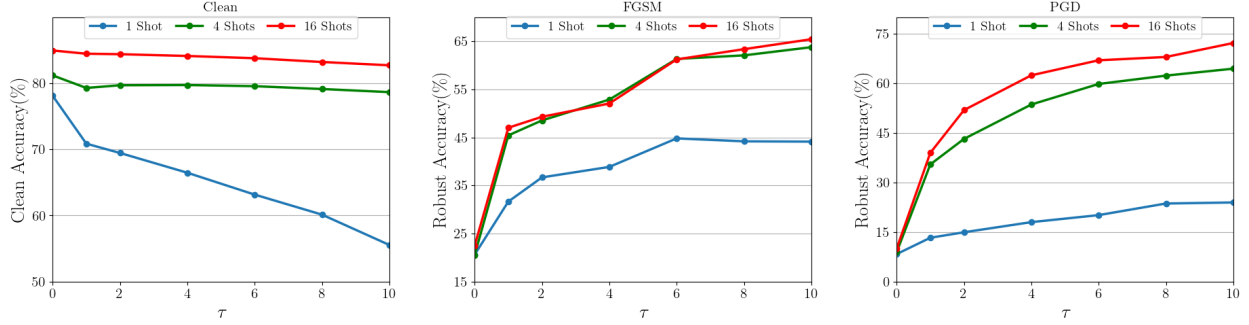


Figure 4: Average performance of AdvCLIP-LoRA with ViT-B/16 backbone on various datasets, showing clean accuracy and robust accuracy for FGSM and PGD attacks with different values of τ .

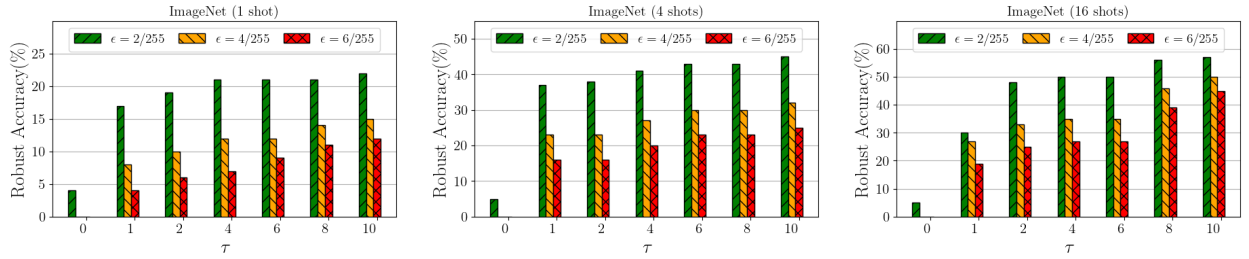


Figure 5: Robust accuracy of AdvCLIP-LoRA with ViT-B/16 backbone on ImageNet with different τ and ϵ values.

rate η_δ then dynamically decays during training, eventually stabilizing at 0.05 after 300 iterations.

Adversarial Attacks. For adversarial training, we define the projection set for updating δ as an ℓ_∞ -ball with a radius of $\epsilon = 10$ across all datasets. To evaluate adversarial robustness, we implement two standard attack methods: FGSM [21] and PGD [23]. For FGSM, we set $\epsilon = 10$, while for PGD, we use $\epsilon = 2$ with a total of 20 attack iterations. Following the setup in [23], the step size for PGD is set to $\alpha = \frac{2.5 \cdot \epsilon}{\text{Number of Iterations}}$.

5.2 Comparative analysis of AdvCLIP-LoRA and CLIP-LoRA

Table 1 presents the experimental results of CLIP-LoRA and AdvCLIP-LoRA with varying values of τ , using the ViT-B/16 backbone. Our findings show that AdvCLIP-LoRA significantly enhances model robustness, increasing FGSM accuracy for a minimum of 11.04% and a maximum of 42.97%, and PGD accuracy for a minimum of 15.67% and a maximum of 62.25%, averaged across all datasets. Specifically, for $\tau = 1$, the model demonstrates improved robustness without a significant impact on clean accuracy (the difference in clean accuracy is less than 22.58% for 1 shot and less than 2.24% for 16 shots, on average). As τ increases, robustness continues to improve; however, this comes at the cost of a slight decrease in clean accuracy. This effect is less prominent for larger shots. It is noteworthy that with 16 shots, the clean accuracy decreases by an average of only 2.24%, while we observe a minimum improvement of 24.55% in the FGSM robustness and 29.00% in the PGD robustness. For clearer comparison, we visualize clean and PGD-robust accuracies for both 4-shot and 16-shot settings across ViT-B/16 and ViT-B/32 backbones in Fig. 3.

Fig. 4 shows the average performance of AdvCLIP-LoRA with ViT-B/16 across the eight datasets.

The results indicate that increasing the number of shots leads to more consistent clean accuracy while yielding disproportionately larger improvements in robust accuracy. Additionally, Fig. 5 illustrates the effect of ϵ in the PGD attack. As expected, larger values of ϵ lead to a reduced robust accuracy on ImageNet. Results for more datasets are provided in Fig. 6 in Appendix A. Further experiments and analysis using the ViT-B/32 backbone are also included in Appendix A.

6 Conclusion

In this work, we presented **AdvCLIP-LoRA**, the first method for enhancing adversarial robustness in CLIP models fine-tuned with LoRA in few-shot settings. By formulating adversarial fine-tuning as a minimax optimization problem, we introduced a theoretically grounded algorithm that provably converges under nonconvex-strong-concavity and smoothness assumptions. Extensive empirical evaluations across eight datasets and two CLIP backbones (ViT-B/16 and ViT-B/32) demonstrate that **AdvCLIP-LoRA** significantly improves robustness against FGSM and PGD attacks, with minimal impact on clean accuracy. Our results highlight the practical feasibility of integrating adversarial robustness into PEFT frameworks for VLMs, opening new directions for adaptation of large pretrained models in resource-constrained and safety-critical scenarios.

References

- [1] A. Radford, J. W. Kim, C. Hallacy, A. Ramesh, G. Goh, S. Agarwal, G. Sastry, A. Askell, P. Mishkin, J. Clark, *et al.*, “Learning transferable visual models from natural language supervision,” in *International conference on machine learning*, pp. 8748–8763, PmLR, 2021.
- [2] C. Jia, Y. Yang, Y. Xia, Y.-T. Chen, Z. Parekh, H. Pham, Q. Le, Y.-H. Sung, Z. Li, and T. Duerig, “Scaling up visual and vision-language representation learning with noisy text supervision,” in *International conference on machine learning*, pp. 4904–4916, PMLR, 2021.
- [3] L. H. Li, P. Zhang, H. Zhang, J. Yang, C. Li, Y. Zhong, L. Wang, L. Yuan, L. Zhang, J.-N. Hwang, *et al.*, “Grounded language-image pre-training,” in *Proceedings of the IEEE/CVF conference on computer vision and pattern recognition*, pp. 10965–10975, 2022.
- [4] L. Yao, R. Huang, L. Hou, G. Lu, M. Niu, H. Xu, X. Liang, Z. Li, X. Jiang, and C. Xu, “Filip: Fine-grained interactive language-image pre-training,” in *International Conference on Learning Representations*.
- [5] R. Zhang, W. Zhang, R. Fang, P. Gao, K. Li, J. Dai, Y. Qiao, and H. Li, “Tip-adapter: Training-free adaption of clip for few-shot classification,” in *European conference on computer vision*, pp. 493–510, Springer, 2022.
- [6] B. Zhu, Y. Niu, Y. Han, Y. Wu, and H. Zhang, “Prompt-aligned gradient for prompt tuning,” in *Proceedings of the IEEE/CVF international conference on computer vision*, pp. 15659–15669, 2023.
- [7] A. Vaswani, “Attention is all you need,” *Advances in Neural Information Processing Systems*, 2017.
- [8] J. Deng, W. Dong, R. Socher, L.-J. Li, K. Li, and L. Fei-Fei, “Imagenet: A large-scale hierarchical image database,” in *2009 IEEE conference on computer vision and pattern recognition*, pp. 248–255, Ieee, 2009.
- [9] S. Chen, C. Ge, Z. Tong, J. Wang, Y. Song, J. Wang, and P. Luo, “Adaptformer: Adapting vision transformers for scalable visual recognition,” *Advances in Neural Information Processing Systems*, vol. 35, pp. 16664–16678, 2022.
- [10] R. Karimi Mahabadi, J. Henderson, and S. Ruder, “Compacter: Efficient low-rank hypercomplex adapter layers,” *Advances in Neural Information Processing Systems*, vol. 34, pp. 1022–1035, 2021.
- [11] S.-A. Rebuffi, H. Bilen, and A. Vedaldi, “Learning multiple visual domains with residual adapters,” *Advances in neural information processing systems*, vol. 30, 2017.
- [12] M. Jia, L. Tang, B.-C. Chen, C. Cardie, S. Belongie, B. Hariharan, and S.-N. Lim, “Visual prompt tuning,” in *European conference on computer vision*, pp. 709–727, Springer, 2022.
- [13] X. L. Li and P. Liang, “Prefix-tuning: Optimizing continuous prompts for generation,” in *Proceedings of the 59th Annual Meeting of the Association for Computational Linguistics and the 11th International Joint Conference on Natural Language Processing (Volume 1: Long Papers)*, Association for Computational Linguistics, 2021.

- [14] E. J. Hu, Y. Shen, P. Wallis, Z. Allen-Zhu, Y. Li, S. Wang, L. Wang, and W. Chen, “Lora: Low-rank adaptation of large language models,” *arXiv preprint arXiv:2106.09685*, 2021.
- [15] T. Dettmers, A. Pagnoni, A. Holtzman, and L. Zettlemoyer, “Qlora: Efficient finetuning of quantized llms,” *Advances in neural information processing systems*, vol. 36, pp. 10088–10115, 2023.
- [16] M. Zanella and I. Ben Ayed, “Low-rank few-shot adaptation of vision-language models,” in *Proceedings of the IEEE/CVF Conference on Computer Vision and Pattern Recognition*, pp. 1593–1603, 2024.
- [17] A. Bulat and G. Tzimiropoulos, “Lasp: Text-to-text optimization for language-aware soft prompting of vision & language models,” in *Proceedings of the IEEE/CVF conference on computer vision and pattern recognition*, pp. 23232–23241, 2023.
- [18] G. Chen, W. Yao, X. Song, X. Li, Y. Rao, and K. Zhang, “Plot: Prompt learning with optimal transport for vision-language models,” in *The Eleventh International Conference on Learning Representations*.
- [19] P. Gao, S. Geng, R. Zhang, T. Ma, R. Fang, Y. Zhang, H. Li, and Y. Qiao, “Clip-adapter: Better vision-language models with feature adapters,” *International Journal of Computer Vision*, vol. 132, no. 2, pp. 581–595, 2024.
- [20] J. Silva-Rodriguez, S. Hajimiri, I. Ben Ayed, and J. Dolz, “A closer look at the few-shot adaptation of large vision-language models,” in *Proceedings of the IEEE/CVF Conference on Computer Vision and Pattern Recognition*, pp. 23681–23690, 2024.
- [21] C. Szegedy, W. Zaremba, I. Sutskever, J. Bruna, D. Erhan, I. Goodfellow, and R. Fergus, “Intriguing properties of neural networks,” *arXiv preprint arXiv:1312.6199*, 2013.
- [22] Z. Zhou, S. Hu, M. Li, H. Zhang, Y. Zhang, and H. Jin, “Advclip: Downstream-agnostic adversarial examples in multimodal contrastive learning,” in *Proceedings of the 31st ACM International Conference on Multimedia*, pp. 6311–6320, 2023.
- [23] A. Madry, A. Makelov, L. Schmidt, D. Tsipras, and A. Vladu, “Towards deep learning models resistant to adversarial attacks,” in *International Conference on Learning Representations*, 2018.
- [24] L. Li, H. Guan, J. Qiu, and M. Spratling, “One prompt word is enough to boost adversarial robustness for pre-trained vision-language models,” in *2024 IEEE/CVF Conference on Computer Vision and Pattern Recognition (CVPR)*, pp. 24408–24419, IEEE Computer Society, 2024.
- [25] J. Zhang, X. Ma, X. Wang, L. Qiu, J. Wang, Y.-G. Jiang, and J. Sang, “Adversarial prompt tuning for vision-language models,” in *ECCV (45)*, 2024.
- [26] X. Jia, S. Gao, S. Qin, K. Ma, X. Li, Y. Huang, W. Dong, Y. Liu, and X. Cao, “Evolution-based region adversarial prompt learning for robustness enhancement in vision-language models,” *arXiv preprint arXiv:2503.12874*, 2025.
- [27] K. Zhou, J. Yang, C. C. Loy, and Z. Liu, “Learning to prompt for vision-language models,” *International Journal of Computer Vision*, vol. 130, no. 9, pp. 2337–2348, 2022.
- [28] K. Zhou, J. Yang, C. C. Loy, and Z. Liu, “Conditional prompt learning for vision-language models,” in *Proceedings of the IEEE/CVF conference on computer vision and pattern recognition*, pp. 16816–16825, 2022.

- [29] H. Yao, R. Zhang, and C. Xu, “Visual-language prompt tuning with knowledge-guided context optimization,” in *Proceedings of the IEEE/CVF conference on computer vision and pattern recognition*, pp. 6757–6767, 2023.
- [30] M. U. Khattak, H. Rasheed, M. Maaz, S. Khan, and F. S. Khan, “Maple: Multi-modal prompt learning,” in *Proceedings of the IEEE/CVF conference on computer vision and pattern recognition*, pp. 19113–19122, 2023.
- [31] Z. Han, C. Gao, J. Liu, J. Zhang, and S. Q. Zhang, “Parameter-efficient fine-tuning for large models: A comprehensive survey,” *Transactions on Machine Learning Research*.
- [32] P. Albert, F. Z. Zhang, H. Saratchandran, C. Rodriguez-Opazo, A. van den Hengel, and E. Abbasnejad, “RandLoRA: Full rank parameter-efficient fine-tuning of large models,” in *The Thirteenth International Conference on Learning Representations*, 2025.
- [33] T. Yu, Z. Lu, X. Jin, Z. Chen, and X. Wang, “Task residual for tuning vision-language models,” in *Proceedings of the IEEE/CVF Conference on Computer Vision and Pattern Recognition*, pp. 10899–10909, 2023.
- [34] Y. Zhou, X. Xia, Z. Lin, B. Han, and T. Liu, “Few-shot adversarial prompt learning on vision-language models,” *Advances in Neural Information Processing Systems*, vol. 37, pp. 3122–3156, 2024.
- [35] P. Liu, W. Yuan, J. Fu, Z. Jiang, H. Hayashi, and G. Neubig, “Pre-train, prompt, and predict: A systematic survey of prompting methods in natural language processing,” *ACM computing surveys*, vol. 55, no. 9, pp. 1–35, 2023.
- [36] T. Lin, C. Jin, and M. Jordan, “On gradient descent ascent for nonconvex-concave minimax problems,” in *International conference on machine learning*, pp. 6083–6093, PMLR, 2020.
- [37] L. Fei-Fei, R. Fergus, and P. Perona, “Learning generative visual models from few training examples: An incremental bayesian approach tested on 101 object categories,” in *2004 conference on computer vision and pattern recognition workshop*, pp. 178–178, IEEE, 2004.
- [38] M. Cimpoi, S. Maji, I. Kokkinos, S. Mohamed, and A. Vedaldi, “Describing textures in the wild,” in *Proceedings of the IEEE conference on computer vision and pattern recognition*, pp. 3606–3613, 2014.
- [39] O. M. Parkhi, A. Vedaldi, A. Zisserman, and C. Jawahar, “Cats and dogs,” in *2012 IEEE conference on computer vision and pattern recognition*, pp. 3498–3505, IEEE, 2012.
- [40] M.-E. Nilsback and A. Zisserman, “Automated flower classification over a large number of classes,” in *2008 Sixth Indian conference on computer vision, graphics & image processing*, pp. 722–729, IEEE, 2008.
- [41] L. Bossard, M. Guillaumin, and L. Van Gool, “Food-101—mining discriminative components with random forests,” in *Computer vision—ECCV 2014: 13th European conference, zurich, Switzerland, September 6-12, 2014, proceedings, part VI 13*, pp. 446–461, Springer, 2014.
- [42] J. Xiao, J. Hays, K. A. Ehinger, A. Oliva, and A. Torralba, “Sun database: Large-scale scene recognition from abbey to zoo,” in *2010 IEEE computer society conference on computer vision and pattern recognition*, pp. 3485–3492, IEEE, 2010.

- [43] K. Soomro, A. R. Zamir, and M. Shah, “Ucf101: A dataset of 101 human actions classes from videos in the wild,” *arXiv preprint arXiv:1212.0402*, 2012.

A Experiment Details

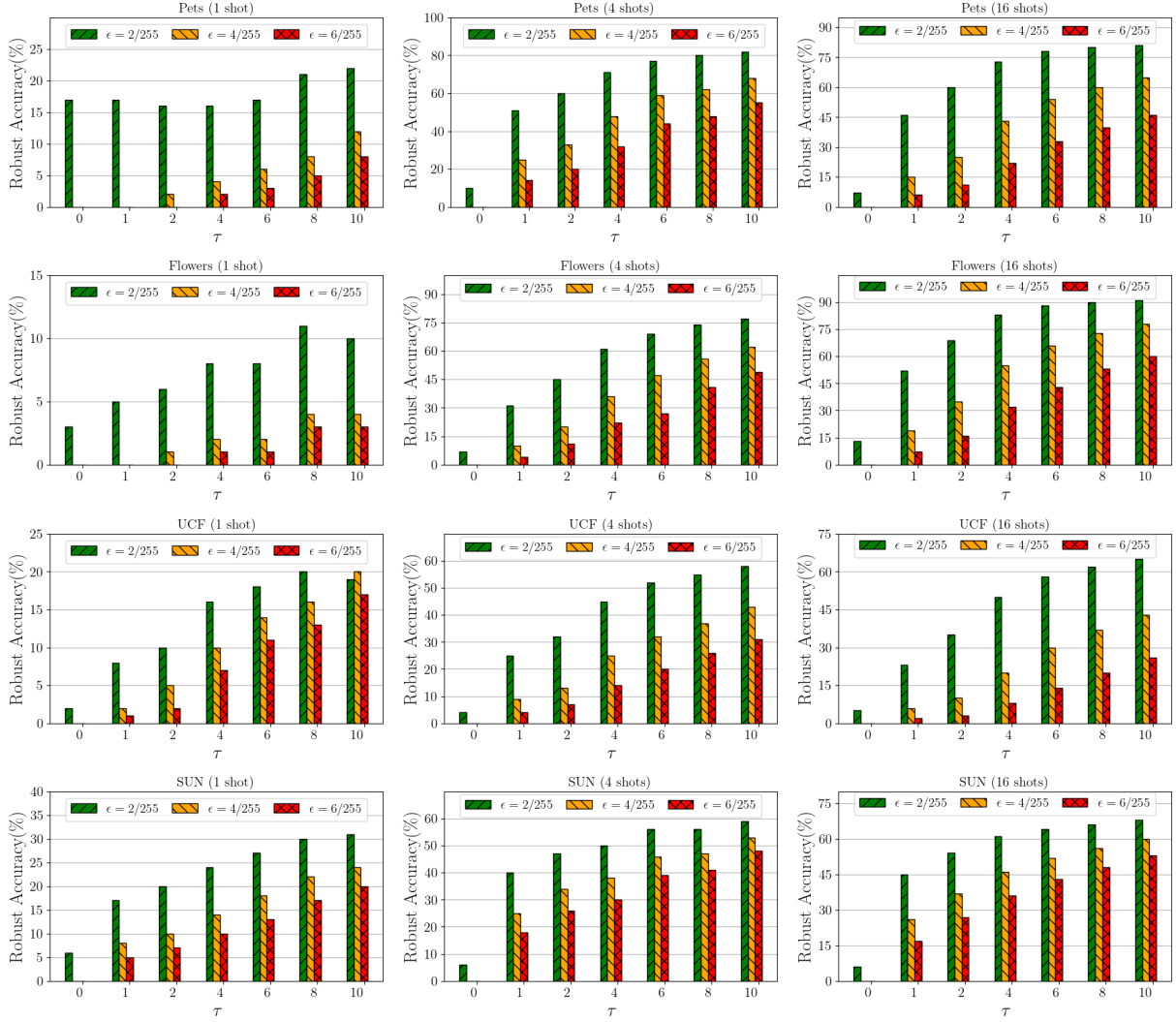


Figure 6: Robust accuracy of AdvCLIP-LoRA with ViT-B/16 backbone on Pets, Flowers, UCF, and SUN datasets with different τ and ϵ values.

Table 2: Detailed results for the 8 datasets with ViT-B/32 as backbone. Top-1 accuracy averaged over 3 random seeds is reported. Highest value is highlighted in **bold**.

Shots	Method	ImageNet			Caltech			DTD			Food		
		Clean	FGSM	PGD	Clean	FGSM	PGD	Clean	FGSM	PGD	Clean	FGSM	PGD
2	CLIP-LoRA	65.70	15.97	8.23	93.54	62.83	42.34	55.46	17.16	9.16	76.53	9.00	4.57
	AdvCLIP-LoRA ($\tau = 1$)	56.97	21.00	11.88	92.11	64.44	40.04	52.03	17.83	5.28	75.68	14.17	6.83
	AdvCLIP-LoRA ($\tau = 2$)	56.73	20.68	11.34	91.89	66.02	41.61	52.05	19.36	6.36	75.70	16.11	8.62
	AdvCLIP-LoRA ($\tau = 4$)	56.32	22.14	12.06	91.94	68.26	44.88	51.16	19.41	6.78	75.71	18.97	10.31
	AdvCLIP-LoRA ($\tau = 6$)	55.45	23.21	12.48	91.63	70.45	46.69	50.26	20.75	7.25	76.11	21.26	11.93
	AdvCLIP-LoRA ($\tau = 8$)	54.87	23.65	12.38	91.76	71.51	48.79	50.22	21.12	7.49	76.32	23.27	13.25
	AdvCLIP-LoRA ($\tau = 10$)	53.46	22.27	10.85	91.58	74.28	52.32	49.33	21.49	8.18	76.35	25.05	14.85
4	CLIP-LoRA	66.43	15.59	8.59	94.44	62.44	42.12	60.18	19.35	10.70	76.18	9.02	4.55
	AdvCLIP-LoRA ($\tau = 1$)	61.60	20.63	13.03	93.90	64.46	43.28	56.40	18.99	7.53	77.30	14.00	7.96
	AdvCLIP-LoRA ($\tau = 2$)	61.44	20.36	12.18	93.75	67.96	51.67	56.68	21.06	9.73	77.52	14.46	10.29
	AdvCLIP-LoRA ($\tau = 4$)	61.44	20.46	12.30	93.81	71.09	55.11	56.58	22.24	12.81	77.88	16.49	13.92
	AdvCLIP-LoRA ($\tau = 6$)	60.49	20.80	12.77	93.47	85.94	59.67	56.17	36.90	15.62	77.96	49.43	17.54
	AdvCLIP-LoRA ($\tau = 8$)	60.22	21.91	12.99	92.82	86.17	62.50	55.32	37.87	18.62	77.40	49.34	23.05
	AdvCLIP-LoRA ($\tau = 10$)	59.10	22.65	13.57	92.94	86.49	65.52	54.34	38.67	22.02	76.91	50.40	27.20
8	CLIP-LoRA	67.28	15.35	8.62	94.46	61.68	43.30	63.36	21.30	13.12	76.90	8.84	4.65
	AdvCLIP-LoRA ($\tau = 1$)	64.19	22.24	14.53	94.67	65.44	49.37	61.17	20.57	9.99	78.03	12.35	8.47
	AdvCLIP-LoRA ($\tau = 2$)	63.93	22.37	14.74	94.63	67.10	58.70	60.78	21.63	14.34	77.90	12.05	13.36
	AdvCLIP-LoRA ($\tau = 4$)	63.76	22.93	16.41	94.54	68.38	68.78	61.11	22.56	22.69	77.55	13.37	22.54
	AdvCLIP-LoRA ($\tau = 6$)	63.50	24.00	17.57	94.28	69.90	74.21	60.05	23.15	27.88	77.29	14.98	27.55
	AdvCLIP-LoRA ($\tau = 8$)	63.22	24.20	18.38	94.38	69.25	77.78	58.81	23.46	30.44	76.94	15.39	31.07
	AdvCLIP-LoRA ($\tau = 10$)	62.74	23.69	18.51	94.39	68.45	79.68	58.91	23.62	32.29	76.57	16.25	33.24
16	CLIP-LoRA	68.43	15.09	9.06	95.50	64.29	47.80	68.62	20.11	16.80	78.00	8.97	5.32
	AdvCLIP-LoRA ($\tau = 1$)	66.24	19.48	13.26	95.84	67.46	55.38	66.90	22.40	12.61	78.55	12.96	10.10
	AdvCLIP-LoRA ($\tau = 2$)	66.08	20.06	15.03	95.40	68.64	66.09	65.84	21.63	19.37	78.41	12.84	16.25
	AdvCLIP-LoRA ($\tau = 4$)	66.08	21.13	15.98	95.39	68.19	75.62	64.89	22.02	29.33	78.09	12.68	24.62
	AdvCLIP-LoRA ($\tau = 6$)	65.39	22.46	17.10	95.46	88.52	80.22	63.91	43.04	34.02	77.75	45.41	28.79
	AdvCLIP-LoRA ($\tau = 8$)	65.63	23.74	21.17	95.31	89.22	82.29	64.01	45.18	38.00	77.44	46.89	32.03
	AdvCLIP-LoRA ($\tau = 10$)	64.06	24.07	17.93	95.28	89.59	84.10	64.77	46.69	39.26	77.08	48.62	35.18
Shots	Method	Pets			Flowers			UCF			SUN		
		Clean	FGSM	PGD	Clean	FGSM	PGD	Clean	FGSM	PGD	Clean	FGSM	PGD
2	CLIP-LoRA	87.43	21.70	16.11	84.40	15.36	10.68	74.07	22.04	7.18	68.71	17.61	8.56
	AdvCLIP-LoRA ($\tau = 1$)	85.70	34.83	16.92	77.71	19.48	8.10	69.41	26.69	8.48	65.45	23.28	13.56
	AdvCLIP-LoRA ($\tau = 2$)	85.14	34.61	18.19	77.16	22.58	10.53	68.06	28.94	8.99	65.22	23.97	13.80
	AdvCLIP-LoRA ($\tau = 4$)	84.90	37.19	22.85	76.12	26.01	12.29	67.48	31.42	10.31	64.96	23.77	14.58
	AdvCLIP-LoRA ($\tau = 6$)	84.67	40.80	26.93	75.78	28.49	13.52	66.56	33.71	11.86	64.64	25.18	14.62
	AdvCLIP-LoRA ($\tau = 8$)	84.39	46.05	31.78	74.83	33.10	16.20	65.64	36.75	13.79	63.30	27.20	16.48
	AdvCLIP-LoRA ($\tau = 10$)	85.07	49.10	34.16	72.71	37.89	19.16	64.19	40.73	16.70	63.59	29.12	17.01
4	CLIP-LoRA	86.43	16.02	11.74	90.21	16.82	13.71	75.65	25.87	7.67	70.20	16.96	8.89
	AdvCLIP-LoRA ($\tau = 1$)	87.87	34.51	27.58	86.32	20.46	16.83	73.43	25.87	10.09	68.93	24.03	15.60
	AdvCLIP-LoRA ($\tau = 2$)	87.87	35.30	33.51	86.26	21.32	19.33	73.39	27.39	12.88	69.22	26.58	16.65
	AdvCLIP-LoRA ($\tau = 4$)	87.82	35.82	37.40	86.26	26.00	30.50	73.57	31.43	16.59	68.92	27.55	17.11
	AdvCLIP-LoRA ($\tau = 6$)	87.80	37.40	46.76	86.29	30.50	32.46	73.72	33.87	23.55	68.88	30.48	19.27
	AdvCLIP-LoRA ($\tau = 8$)	87.56	41.96	53.47	85.82	33.62	39.13	72.75	35.43	26.53	68.40	32.25	20.09
	AdvCLIP-LoRA ($\tau = 10$)	87.52	43.52	56.88	85.34	37.54	43.78	72.28	37.15	28.19	68.47	38.04	23.22
8	CLIP-LoRA	87.61	16.54	10.92	93.29	21.60	18.35	80.46	22.48	9.17	72.18	18.23	9.85
	AdvCLIP-LoRA ($\tau = 1$)	88.71	30.46	24.04	91.76	28.11	21.26	78.64	26.55	11.77	71.73	24.53	16.43
	AdvCLIP-LoRA ($\tau = 2$)	88.75	29.11	35.99	91.91	27.81	34.81	78.67	27.45	18.03	71.71	24.76	17.73
	AdvCLIP-LoRA ($\tau = 4$)	88.63	28.67	50.19	91.65	29.57	51.02	78.35	29.29	27.54	71.86	27.07	20.80
	AdvCLIP-LoRA ($\tau = 6$)	88.65	30.79	57.28	91.76	33.65	58.67	77.53	28.86	33.02	71.57	29.72	23.87
	AdvCLIP-LoRA ($\tau = 8$)	88.53	34.13	61.57	91.20	33.51	63.04	77.22	28.71	37.31	71.39	31.83	26.10
	AdvCLIP-LoRA ($\tau = 10$)	88.26	35.15	64.59	90.91	35.49	65.77	76.36	28.15	39.32	71.10	31.77	28.14
16	CLIP-LoRA	88.43	15.40	10.54	96.39	24.13	22.26	82.86	25.09	10.16	74.09	18.20	10.52
	AdvCLIP-LoRA ($\tau = 1$)	89.67	27.06	23.70	95.22	32.45	30.33	81.18	27.36	13.95	73.77	24.73	17.79
	AdvCLIP-LoRA ($\tau = 2$)	89.66	24.00	35.08	95.75	31.14	48.50	81.18	26.86	21.92	73.46	23.69	20.29
	AdvCLIP-LoRA ($\tau = 4$)	89.69	24.41	50.63	95.93	33.37	62.78	80.99	26.34	31.94	73.52	25.18	23.23
	AdvCLIP-LoRA ($\tau = 6$)	89.56	24.81	57.38	95.49	34.89	70.13	80.49	25.48	37.94	73.61	27.10	25.11
	AdvCLIP-LoRA ($\tau = 8$)	89.27	24.85	61.59	95.25	35.24	74.29	80.49	25.10	41.07	74.09	27.61	29.55
	AdvCLIP-LoRA ($\tau = 10$)	88.83	25.10	64.06	95.20	36.64	77.37	79.56	25.85	43.64	73.65	31.34	31.08

B Convergence Analysis

Before presenting the main theorem, we state several key intermediate lemmas used in the proof. For notational convenience, we denote $\Phi(W := W_0 + BA)$ as $\Phi(BA)$, and use $\Phi(W)$ and $\Phi(BA)$ interchangeably throughout the analysis.

Lemma B.1 *For any matrices $A, B \in \mathbb{R}^{d \times k}$ and $\alpha, \delta > 0$ we have*

$$\begin{aligned} 2\langle A, B \rangle &\leq \delta \|A\|^2 + \delta^{-1} \|B\|^2, \\ \|A + B\|^2 &\leq (1 + \alpha) \|A\|^2 + (1 + \frac{1}{\alpha}) \|B\|^2. \end{aligned} \quad (14)$$

Lemma B.2 *Under Assumptions 4.5 and 4.6, the function Φ is $2\kappa\ell c_B^2$ -smooth with respect to A when B is fixed, and $2\kappa\ell c_A^2$ -smooth with respect to B when A is fixed.*

Proof. First, by the chain rule we notice that

$$\begin{aligned} \nabla_A \Phi(W) &= \nabla_A f(W, \delta^*(W)) = B^T \nabla_W f(W, \delta^*(W)) + \left(\frac{d\delta^*(W)}{dW} \right)^T \underbrace{\nabla_{\delta^*} f(W, \delta^*(W))}_{=0} \\ &= B^T \nabla_W \Phi(W). \end{aligned} \quad (15)$$

Similarly, we have:

$$\nabla_B \Phi(W) = \nabla_W \Phi(W) A^T. \quad (16)$$

Now, we can write

$$\begin{aligned} \|\nabla_A \Phi(BA) - \nabla_A \Phi(BA')\| &= \|B^T \nabla_W \Phi(BA) - B^T \nabla_W \Phi(BA')\| \\ &= \|B\| \|\nabla_W \Phi(BA) - \nabla_W \Phi(BA')\| \\ &\stackrel{(a)}{\leq} c_B(2\kappa\ell) \|BA - BA'\| \\ &\leq 2\kappa\ell c_B^2 \|A - A'\|. \end{aligned} \quad (17)$$

In (a) we used Assumption 4.6 and Proposition 4.7. Similarly, we can prove that Φ is $2\kappa\ell c_A^2$ -smooth with respect to B when A is fixed. \square

Lemma B.3 *The iterates $\{A_t, B_t\}_{t \geq 1}$ in (6) satisfy the following inequality:*

$$\begin{aligned} \mathbb{E} \Phi(B_t A_t) &\leq \mathbb{E} \Phi(B_{t-1} A_{t-1}) - \frac{\eta_w}{2} \left(\mathbb{E} \|\nabla_A \Phi(B_{t-1} A_{t-1})\|^2 + \mathbb{E} \|\nabla_B \Phi(B_{t-1} A_{t-1})\|^2 \right) \\ &\quad + \frac{5\eta_w}{4} \mathbb{E} \|\nabla_A f(B_{t-1} A_{t-1}, \delta_t) - \nabla_A \Phi(B_{t-1} A_{t-1})\|^2 \\ &\quad + \frac{\eta_w}{2} \mathbb{E} \|\nabla_B f(B_{t-1} A_{t-1}, \delta_t) - \nabla_B \Phi(B_{t-1} A_{t-1})\|^2 \\ &\quad + \frac{\kappa\ell(c_A^4 + c_B^4)\eta_w^2 G^2}{M} + \frac{2G^2(2\kappa\ell c_B^2 c_A^4 + G^2)\eta_w^3}{M}. \end{aligned} \quad (18)$$

Proof. Using smoothness for A from Lemma B.2, we can write

$$\begin{aligned}
\mathbb{E}\Phi(B_t A_t) &\leq \mathbb{E}\Phi(B_t A_{t-1}) + \mathbb{E}\langle \nabla_A \Phi(B_t A_{t-1}), A_t - A_{t-1} \rangle + \kappa \ell c_B^2 \eta_w^2 \mathbb{E} \|A_t - A_{t-1}\|^2 \\
&\leq \mathbb{E}\Phi(B_t A_{t-1}) + \mathbb{E}\langle \nabla_A \Phi(B_t A_{t-1}), -\eta_w \nabla_A f(B_{t-1} A_{t-1}, \delta_t) \rangle \\
&\quad + \kappa \ell c_B^2 \eta_w^2 \mathbb{E} \left\| \frac{1}{M} \sum_{i=1}^M \nabla_A F(B_{t-1} A_{t-1}, \delta_t; \xi_i) \right\|^2 \\
&\stackrel{(a)}{\leq} \mathbb{E}\Phi(B_t A_{t-1}) + \frac{\kappa \ell c_B^4 \eta_w^2 G^2}{M} \\
&\quad + \mathbb{E}\langle \nabla_A \Phi(B_t A_{t-1}) - \nabla_A \Phi(B_{t-1} A_{t-1}) + \nabla_A \Phi(B_{t-1} A_{t-1}), -\eta_w \nabla_A f(B_{t-1} A_{t-1}, \delta_t) \rangle \\
&= \mathbb{E}\Phi(B_t A_{t-1}) - \eta_w \mathbb{E}\langle \nabla_A \Phi(B_t A_{t-1}) - \nabla_A \Phi(B_{t-1} A_{t-1}), \nabla_A f(B_{t-1} A_{t-1}, \delta_t) \rangle \\
&\quad - \eta_w \mathbb{E}\langle \nabla_A \Phi(B_{t-1} A_{t-1}), \nabla_A f(B_{t-1} A_{t-1}, \delta_t) \rangle + \frac{\kappa \ell c_B^4 \eta_w^2 G^2}{M} \\
&\stackrel{(b)}{\leq} \mathbb{E}\Phi(B_t A_{t-1}) + 2\eta_w \mathbb{E} \|\nabla_A \Phi(B_t A_{t-1}) - \nabla_A \Phi(B_{t-1} A_{t-1})\|^2 + \frac{\eta_w}{8} \mathbb{E} \|\nabla_A f(B_{t-1} A_{t-1}, \delta_t)\|^2 \\
&\quad - \eta_w \mathbb{E}\langle \nabla_A \Phi(B_{t-1} A_{t-1}), \nabla_A f(B_{t-1} A_{t-1}, \delta_t) - \nabla_A \Phi(B_{t-1} A_{t-1}) + \nabla_A \Phi(B_{t-1} A_{t-1}) \rangle \\
&\quad + \frac{\kappa \ell c_B^4 \eta_w^2 G^2}{M} \\
&\stackrel{(c)}{\leq} \mathbb{E}\Phi(B_t A_{t-1}) + 2\eta_w \mathbb{E} \|\nabla_A \Phi(B_t A_{t-1}) - \nabla_A \Phi(B_{t-1} A_{t-1})\|^2 + \frac{\eta_w}{4} \mathbb{E} \|\nabla_A \Phi(B_{t-1} A_{t-1})\|^2 \\
&\quad + \frac{\eta_w}{4} \mathbb{E} \|\nabla_A \Phi(B_{t-1} A_{t-1}) - \nabla_A f(B_{t-1} A_{t-1}, \delta_t)\|^2 - \frac{3\eta_w}{4} \mathbb{E} \|\nabla_A \Phi(B_{t-1} A_{t-1})\|^2 \\
&\quad + \eta_w \mathbb{E} \|\nabla_A f(B_{t-1} A_{t-1}, \delta_t) - \nabla_A \Phi(B_{t-1} A_{t-1})\|^2 + \frac{\kappa \ell c_B^4 \eta_w^2 G^2}{M} \\
&= \mathbb{E}\Phi(B_t A_{t-1}) + 2\eta_w \mathbb{E} \|\nabla_A \Phi(B_t A_{t-1}) - \nabla_A \Phi(B_{t-1} A_{t-1})\|^2 - \frac{\eta_w}{2} \mathbb{E} \|\nabla_A \Phi(B_{t-1} A_{t-1})\|^2 \\
&\quad + \frac{5\eta_w}{4} \mathbb{E} \|\nabla_A f(B_{t-1} A_{t-1}, \delta_t) - \nabla_A \Phi(B_{t-1} A_{t-1})\|^2 + \frac{\kappa \ell c_B^4 \eta_w^2 G^2}{M}. \tag{19}
\end{aligned}$$

In (a) we applied Assumption 4.4, in (b) we employed the inequality $\langle a, b \rangle \leq \frac{1}{8}\|a\|^2 + 2\|b\|^2$, and in (c) we utilized the inequalities $\langle a, b \rangle \leq \frac{1}{4}\|a\|^2 + \|b\|^2$ and $\|a + b\|^2 \leq 2\|a\|^2 + 2\|b\|^2$. We derive the following bound on the term in the above inequality:

$$\begin{aligned}
\mathbb{E} \|\nabla_A \Phi(B_t A_{t-1}) - \nabla_A \Phi(B_{t-1} A_{t-1})\|^2 &\leq \mathbb{E} \|B_t^T \nabla_W \Phi(B_t A_{t-1}) - B_{t-1}^T \nabla_W \Phi(B_{t-1} A_{t-1})\|^2 \\
&\leq \mathbb{E} \|B_t^T \nabla_W \Phi(B_t A_{t-1}) - B_t^T \nabla_W \Phi(B_{t-1} A_{t-1})\|^2 \\
&\quad + \mathbb{E} \|B_t^T \nabla_W \Phi(B_{t-1} A_{t-1}) - B_{t-1}^T \nabla_W \Phi(B_{t-1} A_{t-1})\|^2 \\
&\leq 2\kappa \ell c_B^2 c_A^2 \mathbb{E} \|B_t - B_{t-1}\|^2 + \mathbb{E} \|B_t^T - B_{t-1}^T\|^2 G^2 \\
&\leq \frac{2\kappa \ell c_B^2 c_A^4 G^2 \eta_w^2}{M} + \frac{G^4 \eta_w^2}{M}. \tag{20}
\end{aligned}$$

If we use (20) in (19), we have

$$\begin{aligned}
\mathbb{E}\Phi(B_t A_t) &\leq \mathbb{E}\Phi(B_t A_{t-1}) - \frac{\eta_w}{2} \mathbb{E} \|\nabla_A \Phi(B_{t-1} A_{t-1})\|^2 \\
&\quad + \frac{5\eta}{4} \mathbb{E} \|\nabla_A f(B_{t-1} A_{t-1}, \delta_t) - \nabla_A \Phi(B_{t-1} A_{t-1})\|^2 \\
&\quad + \frac{\kappa \ell c_B^4 \eta_w^2 G^2}{M} + \frac{4\kappa \ell c_B^2 c_A^4 G^2 \eta_w^3}{M} + \frac{2G^4 \eta_w^3}{M}. \tag{21}
\end{aligned}$$

Using smoothness for B from Lemma B.2, we can write

$$\begin{aligned}
\mathbb{E}\Phi(B_t A_{t-1}) &\leq \mathbb{E}\Phi(B_{t-1} A_{t-1}) + \mathbb{E} \langle \nabla_B \Phi(B_{t-1} A_{t-1}), B_t - B_{t-1} \rangle + \kappa \ell c_A^2 \eta_w^2 \mathbb{E} \|B_t - B_{t-1}\|^2 \\
&\leq \mathbb{E}\Phi(B_{t-1} A_{t-1}) + \mathbb{E} \langle \nabla_B \Phi(B_{t-1} A_{t-1}), -\eta_w \nabla_B f(B_{t-1} A_{t-1}, \delta_t) \rangle \\
&\quad + \kappa \ell c_A^2 \eta_w^2 \mathbb{E} \left\| \frac{1}{M} \sum_{i=1}^M \nabla_B f(B_{t-1} A_{t-1}, \delta_t; \xi) \right\|^2 \\
&\leq \mathbb{E}\Phi(B_{t-1} A_{t-1}) + \frac{\kappa \ell c_A^4 \eta_w^2 G^2}{M} \\
&\quad - \eta_w \mathbb{E} \langle \nabla_B \Phi(B_{t-1} A_{t-1}), \nabla_B f(B_{t-1} A_{t-1}, \delta_t) - \nabla_B \Phi(B_{t-1} A_{t-1}) + \nabla_B \Phi(B_{t-1} A_{t-1}) \rangle \\
&\leq \mathbb{E}\Phi(B_{t-1} A_{t-1}) - \frac{\eta_w}{2} \mathbb{E} \|\nabla_B \Phi(B_{t-1} A_{t-1})\|^2 + \frac{\kappa \ell c_A^4 \eta_w^2 G^2}{M} \\
&\quad + \frac{\eta_w}{2} \mathbb{E} \|\nabla_B f(B_{t-1} A_{t-1}, \delta_t) - \nabla_B \Phi(B_{t-1} A_{t-1})\|^2.
\end{aligned} \tag{22}$$

Summing (21) and (22) yields the desired inequality. \square

Lemma B.4 *Let $\gamma_t = \mathbb{E} \|\delta^*(W_t) - \delta_t\|^2$, the following statement holds true,*

$$\gamma_t \leq \left(1 - \frac{1}{2\kappa}\right) \gamma_{t-1} + \frac{8\kappa^3(c_A^4 + c_B^4)G^2\eta_w^2}{M} + \frac{2G^2}{\ell^2 M}. \tag{23}$$

Proof. Since $f(W_t, \cdot)$ is μ -strongly concave and $\eta_\delta = 1/\ell$, we have [36]

$$\mathbb{E} \|\delta^*(W_{t-1}) - \delta_t\|^2 \leq \left(1 - \frac{1}{\kappa}\right) \gamma_{t-1} + \frac{2G^2}{\ell^2 M}. \tag{24}$$

We can also write

$$\begin{aligned}
\gamma_t &\leq \left(1 + \frac{1}{2(\max\{\kappa, 2\} - 1)}\right) \mathbb{E} \|\delta^*(W_{t-1}) - \delta_t\|^2 \\
&\quad + (1 + 2(\max\{\kappa, 2\} - 1)) \mathbb{E} \|\delta^*(W_t) - \delta^*(W_{t-1})\|^2 \\
&\leq \left(\frac{2\max\{\kappa, 2\} - 1}{2\max\{\kappa, 2\} - 2}\right) \mathbb{E} \|\delta^*(W_{t-1}) - \delta_t\|^2 + 4\kappa \mathbb{E} \|\delta^*(W_t) - \delta^*(W_{t-1})\|^2 \\
&\stackrel{(a)}{\leq} \left(1 - \frac{1}{2\kappa}\right) \gamma_{t-1} + 4\kappa \mathbb{E} \|\delta^*(W_t) - \delta^*(W_{t-1})\|^2 + \frac{2G^2}{\ell^2 M},
\end{aligned} \tag{25}$$

where in (a) we used (24). Since $\delta^*(\cdot)$ is κ -Lipschitz, $\|\delta^*(W_t) - \delta^*(W_{t-1})\| \leq \kappa \|W_t - W_{t-1}\|$. Furthermore, we have

$$\begin{aligned}
\mathbb{E} \|W_t - W_{t-1}\|^2 &= \mathbb{E} \|B_t A_t - B_t A_{t-1} + B_t A_{t-1} - B_{t-1} A_{t-1}\|^2 \\
&\leq 2c_B^2 \mathbb{E} \|A_t - A_{t-1}\|^2 + 2c_A^2 \mathbb{E} \|B_t - B_{t-1}\|^2 \\
&= \frac{2G^2(c_A^4 + c_B^4)\eta_w^2}{M}.
\end{aligned} \tag{26}$$

Using (26) into (25) yields the desired inequality \square

Lemma B.5 *Let $\gamma_t = \mathbb{E} \|\delta^*(W_t) - \delta_t\|^2$, the following statement holds true,*

$$\begin{aligned}
\mathbb{E}\Phi(B_t A_t) &\leq \mathbb{E}\Phi(B_{t-1} A_{t-1}) - \frac{\eta_w}{2} \left(\mathbb{E} \|\nabla_A \Phi(B_{t-1} A_{t-1})\|^2 + \mathbb{E} \|\nabla_B \Phi(B_{t-1} A_{t-1})\|^2 \right) \\
&\quad + \ell^2 \eta_w \left(\frac{5c_B^2 + 2c_A^2}{2} \right) \gamma_{t-1} + \frac{G^2(2.5c_B^2 + c_A^2)\eta_w}{M} + \frac{\kappa \ell (c_A^4 + c_B^4)G^2\eta_w^2}{M} + \frac{2G^2(2\kappa \ell c_B^2 c_A^4 + G^2)\eta_w^3}{M}.
\end{aligned} \tag{27}$$

Proof. Since $\nabla_W \Phi(W_{t-1}) = \nabla_W f(W_{t-1}, \delta^*(W_{t-1}))$, we have

$$\begin{aligned}
& \mathbb{E} \|\nabla_A f(W_{t-1}, \delta^*(W_{t-1})) - \nabla_A f(W_{t-1}, \delta_t)\|^2 \\
&= \mathbb{E} \|B_{t-1}^T \nabla_A f(W_{t-1}, \delta^*(W_{t-1})) - B_{t-1}^T \nabla_A f(W_{t-1}, \delta_t)\|^2 \\
&\leq c_B^2 \ell^2 \mathbb{E} \|\delta^*(W_{t-1}) - \delta_t\|^2 \leq 2c_B^2 \ell^2 \left(\mathbb{E} \|\delta^*(W_{t-1}) - \delta_{t-1}\|^2 + \mathbb{E} \|\delta_t - \delta_{t-1}\|^2 \right) \\
&\leq 2c_B^2 \ell^2 \left(\gamma_{t-1} + \frac{G^2}{\ell^2 M} \right) = 2c_B^2 \ell^2 \gamma_{t-1} + \frac{2c_B^2 G^2}{M}.
\end{aligned} \tag{28}$$

Similarly, we have

$$\mathbb{E} \|\nabla_B f(W_{t-1}, \delta^*(W_{t-1})) - \nabla_B f(W_{t-1}, \delta_t)\|^2 \leq 2c_A^2 \ell^2 \gamma_{t-1} + \frac{2c_A^2 G^2}{M}. \tag{29}$$

Combining (28) and (29) with (18) yields the desired inequality. \square

Theorem B.6 *Under Assumptions 4.4, 4.5, and 4.6, and letting the stepsizes be chosen as*

$$\eta_w = \Theta \left(\min \left\{ \frac{1}{\kappa \ell (c_A^4 + c_B^4)}, \frac{1}{\kappa^2 \ell (c_A^2 + c_B^2)}, \frac{1}{(G^2 + \kappa \ell c_A^4 c_B^2)^{1/2}} \right\} \right), \tag{30}$$

and $\eta_\delta = \Theta(1/\ell)$, the number of iterations required by *AdvCLIP-LoRA* to return an ϵ -stationary point is bounded by

$$\mathcal{O} \left(\frac{4\Delta_\Phi(1/\eta_w) + \kappa \ell^2 (c_A^2 + c_B^2) D^2}{\epsilon^2} \right), \tag{31}$$

where $\Delta_\Phi = \mathbb{E}\Phi(W_0) - \mathbb{E}\Phi(W_{T+1})$. Moreover, the gradient complexity M is bounded by

$$\mathcal{O} \left(\frac{G^2 + \kappa (c_A^2 + c_B^2) G^2}{\epsilon^2} \right). \tag{32}$$

Proof. Performing the inequality in Lemma B.4 recursively and using $\gamma_0 \leq D^2$ from Assumption 4.5 results in

$$\gamma_t \leq \left(1 - \frac{1}{2\kappa}\right)^t D^2 + \left(\frac{8\kappa^3 (c_A^4 + c_B^4) G^2 \eta_w^2}{M} + \frac{2G^2}{\ell^2 M} \right) \left(\sum_{j=0}^{t-1} \left(1 - \frac{1}{2\kappa}\right)^{t-1-j} \right). \tag{33}$$

Combining (33) with (27), we have

$$\begin{aligned}
\mathbb{E}\Phi(W_t) &\leq \mathbb{E}\Phi(W_{t-1}) - \frac{\eta_w}{2} \left(\mathbb{E} \|\nabla_A \Phi(W_{t-1})\|^2 + \mathbb{E} \|\nabla_B \Phi(W_{t-1})\|^2 \right) \\
&\quad + \eta_w \ell^2 \left(\frac{5c_B^2 + 2c_A^2}{2} \right) \left(1 - \frac{1}{2\kappa}\right)^{t-1} D^2 \\
&\quad + \eta_w \ell^2 \left(\frac{5c_B^2 + 2c_A^2}{2} \right) \left(\frac{8\kappa^3 (c_A^4 + c_B^4) G^2 \eta_w^2}{M} + \frac{2G^2}{\ell^2 M} \right) \left(\sum_{j=0}^{t-2} \left(1 - \frac{1}{2\kappa}\right)^{t-2-j} \right) \\
&\quad + \frac{G^2 (2.5c_B^2 + c_A^2) \eta_w}{M} + \frac{\kappa \ell (c_A^4 + c_B^4) G^2 \eta_w^2}{M} + \frac{2G^2 (2\kappa \ell c_B^2 c_A^4 + G^2) \eta_w^3}{M}.
\end{aligned} \tag{34}$$

Summing up (34) over $t = 1, 2, \dots, T+1$ and rearranging, we can write

$$\begin{aligned}
\mathbb{E}\Phi(W_{T+1}) &\leq \mathbb{E}\Phi(W_0) - \frac{\eta_w}{2} \sum_{t=0}^T \left(\mathbb{E} \|\nabla_A \Phi(W_t)\|^2 + \mathbb{E} \|\nabla_B \Phi(W_t)\|^2 \right) \\
&\quad + \eta_w \ell^2 \left(\frac{5c_B^2 + 2c_A^2}{2} \right) D^2 \left(\sum_{t=0}^T \left(1 - \frac{1}{2\kappa} \right)^t \right) \\
&\quad + \eta_w \ell^2 \left(\frac{5c_B^2 + 2c_A^2}{2} \right) \left(\frac{8\kappa^3(c_A^4 + c_B^4)G^2\eta_w^2}{M} + \frac{2G^2}{\ell^2 M} \right) \left(\sum_{t=1}^{T+1} \sum_{j=0}^{t-2} \left(1 - \frac{1}{2\kappa} \right)^{t-2-j} \right) \\
&\quad + \frac{G^2(2.5c_B^2 + c_A^2)\eta_w(T+1)}{M} + \frac{\kappa\ell(c_A^4 + c_B^4)G^2\eta_w^2(T+1)}{M} + \frac{2G^2(2\kappa\ell c_B^2 c_A^4 + G^2)\eta_w^3(T+1)}{M} \\
&\leq \mathbb{E}\Phi(W_0) - \frac{\eta_w}{2} \sum_{t=0}^T \left(\mathbb{E} \|\nabla_A \Phi(W_t)\|^2 + \mathbb{E} \|\nabla_B \Phi(W_t)\|^2 \right) + \kappa\eta_w \ell^2 (5c_B^2 + 2c_A^2) D^2 \\
&\quad + \kappa\eta_w \ell^2 (5c_B^2 + 2c_A^2) \left(\frac{8\kappa^3(c_A^4 + c_B^4)G^2\eta_w^2}{M} + \frac{2G^2}{\ell^2 M} \right) (T+1) \\
&\quad + \frac{G^2(2.5c_B^2 + c_A^2)\eta_w(T+1)}{M} + \frac{\kappa\ell(c_A^4 + c_B^4)G^2\eta_w^2(T+1)}{M} + \frac{2G^2(2\kappa\ell c_B^2 c_A^4 + G^2)\eta_w^3(T+1)}{M}. \tag{35}
\end{aligned}$$

Then, it follows that

$$\begin{aligned}
\frac{1}{T+1} \sum_{t=0}^T \mathbb{E} \|\nabla_{(A,B)} \Phi(W_t)\|^2 &= \frac{1}{T+1} \sum_{t=0}^T \left(\mathbb{E} \|\nabla_A \Phi(W_t)\|^2 + \mathbb{E} \|\nabla_B \Phi(W_t)\|^2 \right) \leq \frac{2(\mathbb{E}\Phi(W_0) - \mathbb{E}\Phi(W_{T+1}))}{\eta_w(T+1)} \\
&\quad + \frac{\kappa\ell^2(10c_B^2 + 4c_A^2)D^2}{T+1} + \kappa\ell^2 (10c_B^2 + 4c_A^2) \left(\frac{8\kappa^3(c_A^4 + c_B^4)G^2\eta_w^2}{M} + \frac{2G^2}{\ell^2 M} \right) + \frac{2G^2(2.5c_B^2 + c_A^2)}{M} \\
&\quad + \frac{2\kappa\ell(c_A^4 + c_B^4)G^2\eta_w}{M} + \frac{4G^2(2\kappa\ell c_B^2 c_A^4 + G^2)\eta_w^2}{M} \\
&\leq \mathcal{O} \left(\frac{\Delta_\Phi}{\eta_w(T+1)} + \frac{\kappa\ell^2(c_A^2 + c_B^2)D^2}{T+1} + \frac{G^2}{M} + \frac{\kappa(c_A^2 + c_B^2)G^2}{M} \right). \tag{36}
\end{aligned}$$

This implies that the number of iterations required by Algorithm 1 to return an ϵ -stationary point is bounded by

$$\mathcal{O} \left(\frac{4\Delta_\Phi(1/\eta_w) + \kappa\ell^2(c_A^2 + c_B^2)D^2}{\epsilon^2} \right), \tag{37}$$

Moreover, the mini-batch size M is bounded by

$$\mathcal{O} \left(\frac{G^2 + \kappa(c_A^2 + c_B^2)G^2}{\epsilon^2} \right), \tag{38}$$

which completes the proof. \square